minerals

Article

Rb$_{1.66}$Cs$_{1.34}$Tb[Si$_{5.43}$Ge$_{0.57}$O$_{15}$]·H$_2$O, a New Member of the OD-Family of Natural and Synthetic Layered Silicates: Topology-Symmetry Analysis and Structure Prediction

Anastasiia Topnikova [1], Elena Belokoneva [1,*], Olga Dimitrova [1], Anatoly Volkov [1] and Dina Deyneko [2]

[1] Geological Faculty, M.V. Lomonosov Moscow State University, Leninskie Gory 1, 119991 Moscow, Russia; nastya_zorina@rambler.ru (A.T.) dimitrova@list.ru (O.D.); toljha@yandex.ru (A.V.)
[2] Chemical Faculty, M.V. Lomonosov Moscow State University, Leninskie Gory 1, 119991 Moscow, Russia; deynekomsu@gmail.com
[*] Correspondence: elbel@geol.msu.ru

Abstract: Crystals of new silicate-germanate Rb$_{1.66}$Cs$_{1.34}$Tb[Si$_{5.43}$Ge$_{0.57}$O$_{15}$]·H$_2$O have been synthesized hydrothermally in a multi-component system TbCl$_3$:GeO$_2$:SiO$_2$ = 1:1:5 at T = 280 °C and P = 100 atm. K$_2$CO$_3$, Rb$_2$CO$_3$ and Cs$_2$CO$_3$ were added to the solution as mineralizers. The crystal structure was solved using single crystal X-ray data: *a* = 15.9429(3), *b* = 14.8407(3), *c* = 7.2781(1) Å, sp. gr. *Pbam*. New Rb,Cs,Tb-silicate-germanate consists of a [Si$_{5.43}$Ge$_{0.57}$O$_{15}$]$_{\infty\infty}$ corrugated tetrahedral layer combined by isolated TbO$_6$ octahedra into the mixed microporous framework as in synthetic K$_3$Nd[Si$_6$O$_{15}$]·2H$_2$O, K$_3$Nd[Si$_6$O$_{15}$] and K$_3$Eu[Si$_6$O$_{15}$]·2H$_2$O with the cavities occupied by Cs, Rb atoms and water molecules. Luminescence spectrum on new crystals was obtained and analysed. A comparison with the other representatives of related layered natural and synthetic silicates was carried out based on the topology-symmetry analysis by the OD (order-disorder) approach. The wollastonite chain was selected as the initial structural unit. Three symmetrical ways of forming ribbon from such a chain and three ways of further connecting ribbons to each other into the layer were revealed and described with symmetry groupoids. Hypothetical structural variants of the layers and ribbons in this family were predicted.

Keywords: RE-silicate-germanate; hydrothermal synthesis; layered silicates; modular approach; wollastonite chain; topology-symmetry analysis; OD theory; structure prediction; luminescence properties

1. Introduction

Si and Ge elements have equal formal charge 4+ and tetrahedral coordination. In the crystal structures, Si and Ge occur together only as the isomorphic substitution Si-Ge in tetrahedra. Both elements are present isomorphically in the minerals sanbornite, milarite, albite, perrierite, farmakosiderite, garnet, titanite, and zeolite analogues [1]. Lone pair heavy metals act together with different anionic units containing mixing components. Such an approach is actually used in materials design to result in promising properties. There are no silicate-germanates with Tb in the nature or synthetic compounds according to [1,2]. However, there are a lot of original synthetic Tb-silicates with different anionic radicals [2,3]: ortho- NaTb$_9$(SiO$_4$)$_6$O$_2$ [4], KTb$_9$(SiO$_4$)$_6$O$_2$ and Cd$_2$Tb$_8$(SiO$_4$)$_6$O$_2$ [5] (structural type of apatite), Na$_5$Tb$_4$(OH)[SiO$_4$]$_4$ [6]; diortho- Tb$_2$Si$_2$O$_7$ [7], K$_3$TbSi$_2$O$_7$ [8], Tb$_4$S$_3$Si$_2$O$_7$ [9]; triortho- K$_3$TbSi$_3$O$_8$(OH)$_2$ [10]; tetraortho-groups Ba$_2$Tb$_2$Si$_4$O$_{13}$ [11]; six-membered rings Na$_3$Tb$_3$Si$_6$O$_{18}$·H$_2$O (synthetic gerenite) [12]; chains—unbranched Rb$_2$TbGaSi$_4$O$_{12}$ [13], wollastonite Na$_2$Tb$_{1.08}$Ca$_{2.92}$Si$_6$O$_{18}$H$_{0.8}$ [14] and spiral Na$_3$TbSi$_3$O$_9$·3H$_2$O [15]; layers in Cs$_3$TbSi$_4$O$_{10}$F$_2$ [16] and K$_{7.04}$Tb$_3$Si$_{12}$O$_{32.02}$·1.36H$_2$O [17]; sheets in Cs$_3$TbSi$_8$O$_{19}$·2H$_2$O [18] and Na$_4$K$_2$Tb$_2$Si$_{16}$O$_{38}$·10H$_2$O [19]. For some of these compounds, the luminescence properties were investigated [6,10,13–15,18,19].

Silicate crystal structures with the layers are presented [20,21] as a result of condensation of various chains. The formation of chains, layers, or frameworks by linking tetrahedra by the symmetry elements are partially addressed in a monograph [20], where the chains of Ba-silicates and symmetry elements responsible for their formation are identified. Important aspects of the modular approach and OD description of crystal structures were analyzed in [22]. For careful analysis of the similarities and differences in crystal structures, it is necessary to separate building units or modules which may be similar in different minerals, for example, layers in micas. The use of symmetry, a fundamental concept in crystallography, is a key tool for the description of structural families and for the construction of anionic radicals. Such an approach was suggested in [23] for layered ordered crystal structures in which a significant disorder component may be presented (OD theory). The local symmetry of layers or rods leads to structural variants of their conjugation and allows to predict new crystal structures. In the OD family, sursassite-pumpellyite-ardennite, the fourth member, was predicted and confirmed by high-resolution electron microscopy [24]. Strict symmetric rules dictate all possibilities in real or hypothetical crystal structures. The symmetry approach, based on the principles of OD theory [23], was developed for the borates [25] at all levels of condensation from the initial isolated tetrahedron to the chain, layer, and framework anionic units and described by groupoids of different ranks. As mentioned in the investigation of the crystal structure of the chain diborate $GdH[B_2O_5]$ [26], the results are the same for borates, silicates, and other tetrahedral radicals. Thus, the borate chain in vimsite $Ca[B_2O_2(OH)_4]$ is identical to the pyroxene chain. The formation of ribbons, layers, and frameworks in the well-known silicates are considered in [26]. The letters U (upward) and D (downward), which are commonly used in the literature for the description of tetrahedral anionic groups (chains, layers, and frameworks) actually reflects the absence or presence of inversion symmetry elements [27]. Two-chain ribbons are present in palygorskite $Mg_5[Si_4O_{10}]_2(OH)_2 \cdot 8H_2O$, and three-chain ribbons in sepiolite $Mg_4[Si_6O_{15}](OH)_2 \cdot 6H_2O$. In both minerals, pyroxene chains are related by the symmetry elements m_y, -1, m_y, -1 ... (palygorskite) or m_y, m_y, 2_x, m_y, m_y, 2_x ... (sepiolite) [26]. The crystal structure of α-celsian $Ba[Al_2Si_2O_8]$ demonstrates next step of condensation: nonpolar double-decker sheets are formed of polar mica-like layers multiplied by the mirror plane m_z via sharing of the apical vertices of the tetrahedra.

Synthesis of a new Rb,Cs,Tb-silicate-germanate, its structure solution and crystal chemical comparison with known related natural and synthetic silicates led us to using topology-symmetry analysis of OD theory. The following rubricating of known and predicted layered crystal structures is presented in this work. Luminescence properties are also characterized.

2. Materials and Methods

### 2.1. Synthesis of Crystals

The crystals of a new Rb,Cs,Tb-silicate-germanate were synthesized by a hydrothermal method in the system, containing oxide and chloride components in the mass ratio $TbCl_3:GeO_2:SiO_2 = 1:1:5$ that corresponds to 1.0 g (0.003 mol) $TbCl_3$, 1.0 g (0.001 mol) GeO_2 and 5.0 g (0.017 mol) SiO_2. All the reagents were of analytical grade. The mass ratio of solid and liquid phases was 1:5. K_2CO_3, Rb_2CO_3 and Cs_2CO_3 were added at the solution as mineralizers. The phase formation occurred at a pH 3 (measured after the completion of the reaction). The synthesis was carried out at the temperature of 280 °C and pressure of 100 atm. A standard autoclave (capacity 5 to 6 cm^3) lined with Teflon was used. The characteristics of experiment were limited by the kinetics of the hydrothermal reactions and the instrumental capabilities. The reaction went to completion during heating for 18 to 20 days; followed by cooling to room temperature for over 24 h. The grown crystals were isolated by filtering the stock solution, washed with water and finally dried at room temperature. The small colorless transparent prismatic crystals, splices and brushes of crystals were found in the reaction products. The yield of the crystals was about 50 vol.%. Determination of the unit cell parameters on single crystals was performed using pre-

experiment on Xcalibur S diffractometer (CCD area detector; graphite-monochromated Mo-K$_\alpha$ radiation). The chemical composition was determined using a Jeol JSM-6480LV scanning electronic microscope combined with WDX analysis (Jeol, Osaka, Japan). The qualitative test revealed the presence of Tb, Cs, Rb, Si, Ge and O.

2.2. Luminescence Study

Photoluminescence emission (PL) and excitation (PLE) spectra were recorded on an Agilent Cary Eclipse fluorescence spectrometer (Agilent Technology, Malaysia) with a 75 kW xenon light source (pulse length τ = 2 µs, pulse frequency ν = 80 Hz, wavelength resolution 0.5 nm; PMT Hamamatsu R928). For correct determination of photoluminescent properties, the measurements were performed on three portions of the crystals. The photoluminescence spectra of all samples were obtained under similar experimental conditions to compare the relative emission intensities and reduce the error. The experiment showed complete reproduction of the photoluminescence data for these three portions. The obtained spectra were corrected for the sensitivity of the spectrometer.

In Figure 1a, the PLE spectrum of $Rb_{1.66}Cs_{1.34}Tb[Si_{5.43}Ge_{0.57}O_{15}]\cdot H_2O$ is shown. According to the results, the Tb^{3+} ion can be excited in different ways: within intraconfigural $4f^8$ transitions, and by interconfigural $4f^8$–$4f^75d^1$ transition [28]. Several bands at 300 to 500 nm are attributed to f-f transitions of Tb^{3+} ions from the $^7F_6$ ground state to the $^5H_6$ (303 nm), $^5H_7$ (320 nm), $^5L_9$ (360 nm), $^5D_3$ (378 nm) and $^5D_4$ (480 nm). The most intensive $^5D_3$ transition was not split.
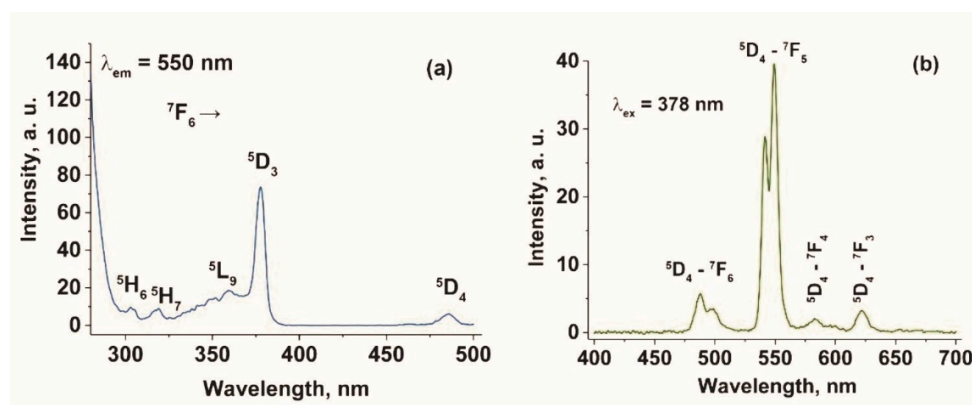
Figure 1. $Rb_{1.66}Cs_{1.34}Tb[Si_{5.43}Ge_{0.57}O_{15}]\cdot H_2O$: PLE spectrum (**a**) and PL spectrum at λ_{exc} = 378 nm (**b**).

In Figure 1b, the PL spectrum of $Rb_{1.66}Cs_{1.34}Tb[Si_{5.43}Ge_{0.57}O_{15}]\cdot H_2O$ controlled at λ_{exc} = 378 nm is shown. The spectrum consists of $^5D_4 \rightarrow {}^7F_J$ (J = 3–6) optical transitions of Tb^{3+} ion. The emission from the hypersensitive $^5D_4$–$^7F_5$ transition at 540 nm is predominant. There was no emission from the higher lying $^5D_3$ level to ^7F_J states (Figure 1b). Generally, the absence of these transitions is due to the presence of efficient cross-relaxation processes [29]. The deactivation in the $^5D_3$ emitting state such as $^5D_3 \rightarrow {}^5D_4$ and $^7F_6 \rightarrow {}^7F_0$ or $^5D_3 \rightarrow {}^7F_0$ and $^7F_6 \rightarrow {}^5D_4$ [30,31] is observed since the concentration of Tb^{3+} is relatively high. The main peak is split into two Stark components. This, apparently, is due to the presence of two non-equivalent positions occupied by Tb^{3+} in the crystal structure. Only the $^5D_4$–^7F_J (J = 3–6) transition lines have a measurable intensity. It was noted that the luminescence intensity of the $^5D_4 \rightarrow {}^7F_3$ transition could become comparable to that of the main green $^5D_4 \rightarrow {}^7F_5$ transition of Tb^{3+}, when the crystal field is strong [32]. In $Rb_{1.66}Cs_{1.34}Tb[Si_{5.43}Ge_{0.57}O_{15}]\cdot H_2O$ the $^5D_4 \rightarrow {}^7F_3$ compared to $^5D_4 \rightarrow {}^7F_5$ is less, by approximately 10 times. So, the studied crystal has a low crystal field strength. In addition, the ratio between the $^5D_4 \rightarrow {}^7F_5$ transition (green band at 490 nm) to the $^5D_4 \rightarrow {}^7F_6$ transition (blue band at 540 nm) is known as green-to-blue fluorescence factor (G/B) [33]. The G/B (Tb^{3+}) determines the asymmetry of the local environment around the Tb^{3+} ions and character bonding (covalent/ionic) between Tb^{3+} and O^{2-}. The G/B factor for Tb^{3+}

ions in $Rb_{1.66}Cs_{1.34}Tb[Si_{5.43}Ge_{0.57}O_{15}]\cdot H_2O$ is 5.01 has been calculated. The obtained value is rather high, which suggests more covalent character of the bonding between terbium and oxygen ions. This is due to the presence of heavy rubidium and cesium atoms in the crystal composition.

3. Results

Structure Solving and Description

A small colorless transparent short-prismatic crystal with a size of $0.10 \times 0.05 \times 0.04$ mm was selected for the single-crystal X-ray study. The diffraction experiment was carried out on an Xcalibur-S diffractometer (Oxford Diffraction, Oxford, UK) with a graphite-monochromatized Mo-K_α radiation source ($\lambda = 0.71073$ Å) and a CCD detector (ω scanning mode). The data were integrated using the CrysAlis Pro Agilent Technologies (v.1.1713735. 2014) software [34] and corrected for the Lorentz and polarization factors. The refined orthorhombic unit-cell parameters are $a = 15.9429(3)$, $b = 14.8407(3)$, $c = 7.2781(1)$ Å, $V = 1722.03(6)$ Å^3. A structural model was found by the direct method determination using SHELXS [35] within the WinGX v2018.3 [36] software in the suggested space group *Pbam* in agreement with the systematically absent reflections. At the first step, Tb1, Tb2, Rb1, Rb2, Cs1, Si and several of O sites were found. The remaining O sites were detected in different Fourier syntheses and were introduced in the model. As the temperature displacement parameters for all Si sites and Rb2 site were decreased, a small amount of Ge was isomorphically added in the Si sites (($Si_{0.93}Ge_{0.07}$)1, ($Si_{0.88}Ge_{0.12}$)2, ($Si_{0.91}Ge_{0.09}$)3, ($Si_{0.92}Ge_{0.08}$)4) and Cs—in Rb2 site ($Rb_{0.66}Cs_{0.34}$)2 which significantly improved the *R*-factor. The occupations of these sites were found first by changing them step by step in a search for the minimum *R*-factor with the control of the temperature displacement parameters. After that, we applied the procedure of the refinement of tetrahedral position occupations and (Rs,Cs)2 position occupations, which made it possible to improve the result. The O11 atom was identified as the oxygen of a water molecule based on Pauling's bond valence distribution [37] (Table 1). The resulting chemical formula is $Rb_{1.66}Cs_{1.34}Tb[Si_{5.43}Ge_{0.57}O_{15}]\cdot H_2O$, Z = 4. The structural model in a space group *Pbam* was refined using the least squares procedure in anisotropic approximation of the atomic displacements and with the refinement of the weighting scheme using SHELXL [38]. The absorption of crystal was not corrected because it was negligible $\mu r_{max} = 0.63$ and did not influence the result. Crystallographic data, atomic coordinates and selected bonds are presented in Tables 2–4. CCDC CSD 2,062,486 contains crystallographic data for this paper. These data can be obtained free of charge via www.ccdc.cam.ac.uk/data_request/cif (accessed on 24 March 2021). Illustrations were produced using ATOMS (v. 5.1) [39] and CORELDRAW (v. 21.0.0.593, 2019) programs.

Table 1. Pauling's balance of valences for $Rb_{1.66}Cs_{1.34}Tb[Si_{5.43}Ge_{0.57}O_{15}]\cdot H_2O$.

	Tb1³⁺ C.N. = 6 0.25*	Tb2³⁺ C.N. = 6 0.25*	Cs1⁺ C.N. = 11 0.5*	Rb1⁺ C.N. = 9 0.5*	(Rb,Cs2)⁺ C.N. = 7 0.5*	T1⁴⁺ C.N. = 4 0.5*	T2⁴⁺ C.N. = 4 1.0*	T3⁴⁺ C.N. = 4 1.0*	T4⁴⁺ C.N. = 4 0.5*	Σexp	Σtheor
O1²⁻ 0.5 *			0.045	0.056				1.0		−1.1	−1.0
O2²⁻ 0.5 *					0.071	0.5			0.5	−1.071	−1.0
O3²⁻ 1.0 *		0.125 × 4	0.045 × 4		0.071 × 2			1.0		−1.825	−2.0
O4²⁻ 1.0 *	0.125 × 4			0.056 × 4			1.0			−1.722	−2.0
O5²⁻ 1.0 *				0.056 × 2		0.5 × 2		1.0		−2.111	−2.0
O6²⁻ 1.0 *					0.071 × 2		1.0	1.0		−2.143	−2.0
O7²⁻ 0.5 *		0.125 × 2	0.045 × 2		0.071				0.5	−0.912	−1.0
O8²⁻ 1.0 *			0.045 × 2				1.0		0.5 × 2	−2.091	−2.0
O9²⁻ 0.5 *	0.125 × 2				0.071	0.5				−0.821	−1.0
O10²⁻ 0.5 *			0.045	0.056			1.0			−1.1	−1.0
O11w²⁻ 0.5 *			0.045	0.056						−0.1	0
Σ	+0.75	+0.75	+0.5	+0.5	+0.5	+2	+4	+4	+2	15	15

* These values correspond to multiplicities scaled to common position multiplicity equal to 1.0.

Table 2. Crystal data and structure refinement for $Rb_{1.66}Cs_{1.34}Tb[Si_{5.43}Ge_{0.57}O_{15}]\cdot H_2O$.

Formula	$Rb_{1.66}Cs_{1.34}Tb[Si_{5.43}Ge_{0.57}O_{15}]\cdot H_2O$
formula weight (g/mol)	930.48
T (K)	293(2)
crystal system	Orthorhombic
space group, Z	*Pbam*, 4
a (Å)	15.9429(3)
b (Å)	14.8407(3)
c (Å)	7.2781(1)
V (Å^3)	1722.03(6)
crystal size (mm)	$0.10 \times 0.05 \times 0.04$
ρ_{calc} (g/cm^3)	3.532
μ (mm^{-1})	12.610
F(000)	1677
wavelength (Å)	0.71073
θ range/deg.	2.75–30.78
limiting indices	$-22 \le h \le 22, -21 \le k \le 20, -10 \le l \le 10$
refl. collected/unique	28316/2756 [R_{int} = 0.0695]
completeness to theta	99.9
data/restraints/parameters	2756/0/143
GOF	1.187
R_1, wR_2 [1] [$I > 2\sigma(I)$]	0.0541, 0.0885
R_1, wR_2 (all data) [1]	0.0670, 0.0926
$\Delta\rho_{max}$ and $\Delta\rho_{min}$ (e Å^{-3})	1.726 and -2.318

[1] $R(F) = \sum||F_o| - |F_c||/\sum|F_o|$ and $wR_2 = [\sum w(F_o^2 - F_c^2)^2/\sum w(F_o^2)^2]^{1/2}$ for $F_o^2 > 2\sigma(F_o^2)$.

Table 3. Atomic coordinates and atomic displacement parameters (U, Å^2) for $Rb_{1.66}Cs_{1.34}Tb[Si_{5.43}Ge_{0.57}O_{15}]\cdot H_2O$. U_{eq} is defined as one third of the trace of the orthogonalized U_{ij} tensor.

Atoms	Wyckoff Position, Point Symm.	S.o.f.	X	Y	Z	U_{eq}
Cs1	4g, m	1.0	0.1306(1)	0.5459(1)	0	0.0255(2)
Rb1	4h, m	1.0	0.2830(1)	0.8920(1)	0.5	0.0408(4)
(Rb, Cs)2	4g, m	0.66, 0.34	0.4222(1)	0.4033(1)	0	0.0250(2)
Tb1	2b, 2/m	1.0	0.5	0.5	0.5	0.00832(14)
Tb2	2d, 2/m	1.0	0	0.5	0.5	0.00750(14)
(Si, Ge)1	4h, m	0.93, 0.07	0.0874(1)	0.7829(2)	0.5	0.0083(7)
(Si, Ge)2	8i, 1	0.88, 0.12	0.3535(1)	0.6345(1)	0.7838(2)	0.0077(5)
(Si, Ge)3	8i, 1	0.91, 0.09	0.0395(1)	0.3024(1)	0.2181(2)	0.0087(5)
(Si, Ge)4	4h, m	0.92, 0.08	0.2068(1)	0.6291(2)	0.5	0.0060(7)
O(1)	4g, m	1.0	0.0165(5)	0.2918(5)	0	0.0192(16)
O(2)	4h, m	1.0	0.1804(4)	0.7355(4)	0.5	0.0139(15)
O(3)	8i,1	1.0	0.0526(3)	0.4042(3)	0.2791(7)	0.0150(10)
O(4)	8i,1	1.0	0.4291(3)	0.5701(4)	0.7326(8)	0.0176(11)
O(5)	8i, 1	1.0	0.0392(3)	0.7465(4)	0.3168(7)	0.0184(11)
O(6)	8i, 1	1.0	0.1258(3)	0.2425(3)	0.2554(7)	0.0141(10)
O(7)	4h, m	1.0	0.1292(4)	0.5630(5)	0.5	0.0134(14)
O(8)	8i, 1	1.0	0.2653(3)	0.6115(4)	0.6809(7)	0.0189(11)
O(9)	4h, m	1.0	0.0990(4)	0.8882(5)	0.5	0.0142(15)
O(10)	4g, m	1.0	0.3262(5)	0.6260(6)	0	0.0187(16)
O(11)w	4g, m	1.0	0.2446(9)	0.3400(10)	0	0.079(4)

Table 4. Selected interatomic distances for $Rb_{1.66}Cs_{1.34}Tb[Si_{5.43}Ge_{0.57}O_{15}]\cdot H_2O$.

Atoms	Bonds (Å)	Atoms	Bonds (Å)
$Tb1O_6$ Octahedron		**$Tb2O_6$ Octahedron**	
Tb1-O4 x4	2.286(5)	Tb2-O7 ×2	2.262(7)
Tb1-O9 ×2	2.290(7)	Tb2-O3 ×4	2.304(5)
Average	2.287	Average	2.290
$(Si,Ge)1O_4$ Tetrahedron		**$(Si,Ge)2O_4$ Tetrahedron**	
(Si,Ge)1-O9	1.573(7)	(Si,Ge)2-O4	1.582(5)
(Si,Ge)1-O5 ×2	1.632(5)	(Si,Ge)2-O8	1.629(5)
(Si,Ge)1-O2	1.640(7)	(Si,Ge)2-O10	1.637(3)
Average	1.619	(Si,Ge)2-O6	1.662(5)
$(Si,Ge)3O_4$ Tetrahedron		Average	1.628
(Si,Ge)3-O3	1.588(5)	**$(Si,Ge)4O_4$ Tetrahedron**	
(Si,Ge)3-O5	1.617(5)	(Si,Ge)4-O7	1.579(7)
(Si,Ge)3-O1	1.637(3)	(Si,Ge)4-O8 x2	1.634(5)
(Si,Ge)3-O6	1.660(5)	(Si,Ge)4-O2	1.635(7)
Average	1.626	Average	1.621

The new crystal structure of $Rb_{1.66}Cs_{1.34}Tb[Si_{5.43}Ge_{0.57}O_{15}]\cdot H_2O$ consists of mixed (Si, Ge) tetrahedra (Table 3) which are combined into the corrugated layer $[Si_{5.68}Ge_{0.32}O_{15}]_{\infty\infty}$ parallel to *ac* containing four-, six- and eight-membered rings. The isolated TbO_6 centrosymmetric octahedra (Table 4) connected with (Si, Ge) tetrahedral layers into the mixed microporous framework. Rb, Cs atoms and water molecules fill the channels of the framework (Figure 2a,b).
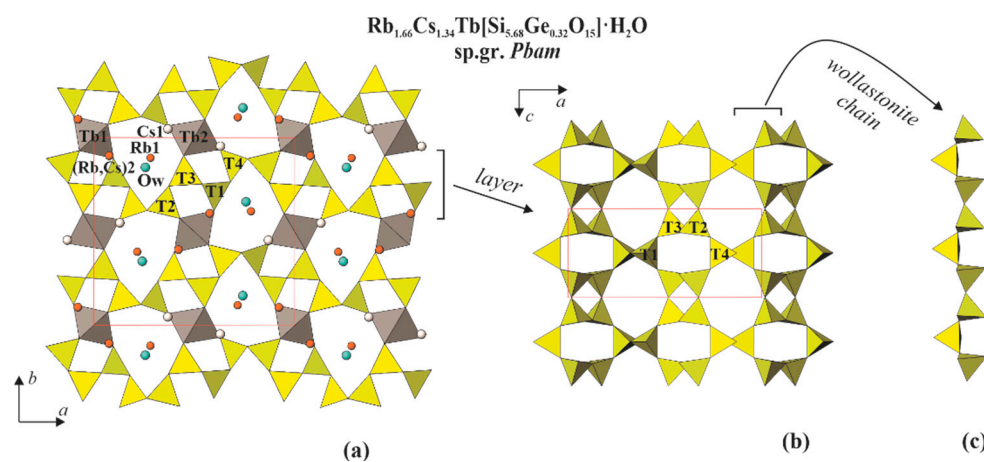
Figure 2. Crystal structure of $Rb_{1.66}Cs_{1.34}Tb[Si_{5.43}Ge_{0.57}O_{15}]\cdot H_2O$: mixed framework in *ab*-projection (**a**), Si-O tetrahedral layer in *ac*-projection (**b**) and isolated wollastonite chain (**c**).

4. Discussion

4.1. Structural Comparison with the Related Layered Silicates

Polytypic relations between isochemical alkali-REE layer silicates and sazhinite were analyzed in [40]. Multiring tetrahedral sheets for four crystal structures: sazhinite $Na_2Ce[Si_6O_{14}(OH)_2]\cdot nH_2O$ [41], $Na_{2.74}K_{0.26}Ce[Si_6O_{15}]\cdot 2H_2O$ [42], $Na_{2.4}Ce[Si_6O_{15}]\cdot 2H_2O$ [43], $K_3Nd[Si_6O_{15}]\cdot 2H_2O$ [44] were analyzed, emphasizing the presence of a xonotlite-like ribbon. Polytypic relations were derived for the compounds and the crucial role of large K cations was found in forming crystal structures. Some symmetry elements were described: *m* mirror plane for sazhinite structure type, *a* glide for $Na_{2.4}Ce[Si_6O_{15}]\cdot 2H_2O$. Diffraction features, which present some diffusion effects and spurious reflections, were fixed on reciprocal lattice *h0l* and *h1l*.

The crystal structure of a new member of the family, $Rb_{1.66}Cs_{1.34}Tb[Si_{5.43}Ge_{0.57}O_{15}]\cdot H_2O$, is close to the layered $K_3Nd[Si_6O_{15}]\cdot 2H_2O$ [44], $K_3Nd[Si_6O_{15}]$ [45] and $K_3Eu[Si_6O_{15}]\cdot 2H_2O$

(symmetry decrease is caused by the displacement of some atoms from the *m*-plane) [46] (Table 5). All the compounds have identical mixed frameworks consisting of Si-O tetrahedral layers combined with isolated REEO$_6$-octahedra. The new crystal structure differs from these only by the substitution of Rb, Cs for K and the amount of water molecules. Different filling of voids is a characteristic feature of this structural family up to differences in individual crystals of the same mineral sample. Silicate K$_3$Eu[Si$_6$O$_{13}$(OH)$_4$]·2H$_2$O [46] contains ribbon [Si$_6$O$_{13}$(OH)$_4$]$_\infty$ instead of layer (Figure 3a). The similar ribbon as in the latter crystal structure is presented in the layers of all former silicates including the new member. Ribbons are multiplied into the layer along the *a*-axis by inversion center (Figure 3b).

Table 5. The main crystallographic characteristics of the family structures.

Chemical Formula	Space Group	Unit Cell Parameters, Å	Reference
Rb$_{1.66}$Cs$_{1.34}$Tb[Si$_{5.43}$Ge$_{0.57}$O$_{15}$]· H$_2$O	*Pbam*	*a* = 15.943 *b* = 14.841 *c* = 7.278	[this work]
K$_3$Nd[Si$_6$O$_{15}$]·2H$_2$O	*Pbam*	*a* = 16.008 *b* = 15.004 *c* = 7.279	[44]
K$_3$Nd[Si$_6$O$_{15}$]	*Pbam*	*a* = 16.011 *b* = 14.984 *c* = 7.276	[45]
K$_3$Eu[Si$_6$O$_{15}$]·2H$_2$O	*P*2$_1$2$_1$2	*a* = 14.852 *b* = 15.902 *c* = 7.243	[46]
Na$_2$Ce[Si$_6$O$_{14}$(OH)$_2$]·nH$_2$O Ce-sazhinite	*Pmm*2	*a* = 7.500 *b* = 15.620 *c* = 7.350	[41]
Na$_3$La[Si$_6$O$_{15}$]·2H$_2$O La-sazhinite	*Pmm*2	*a* = 7.415 *b* = 15.515 *c* = 7.164	[47]
β-K$_3$Nd[Si$_6$O$_{15}$]	*Bb*2$_1$*m*	*a* = 14.370 *b* = 15.518 *c* = 14.265	[44]
Na$_{2.4}$Ce[Si$_6$O$_{15}$]·2H$_2$O	*Pman*	*a* = 7.309 *b* = 14.971 *c* = 7.135	[43]
NaNd[Si$_6$O$_{13}$(OH)$_2$]·H$_2$O	*Cmm*2	*a* = 30.870 *b* = 7.387 *c* = 7.120	[48]
NaNd[Si$_6$O$_{15}$]·2H$_2$O	*Cmm*2	*a* = 7.385 *b* = 30.831 *c* = 7.117	[49]
Na$_{2.74}$K$_{0.26}$Ce[Si$_6$O$_{15}$]·2H$_2$O	*Cmm*2	*a* = 7.413 *b* = 30.965 *c* = 7.167	[42]
Na$_3$La[Si$_6$O$_{15}$]·2.25H$_2$O	*Cmm*2	*a* = 7.415 *b* = 31.008 *c* = 7.153	[42]
Na$_{2.72}$K$_{0.25}$LaSi$_6$O$_{15}$·2.25H$_2$O	*Cmm*2	*a* = 7.422 *b* = 31.039 *c* = 7.196	[42]

The crystal structure of sazhinite Na$_2$Ce[Si$_6$O$_{14}$(OH)$_2$]·nH$_2$O [41] (Na$_3$La[Si$_6$O$_{15}$]· 2H$_2$O [47]) (Table 5) is similar to the Rb,Cs,Tb-silicate-germanate mixed framework and configuration of the corrugated tetrahedral layer with four-, six- and eight-membered rings (Figures 2a and 4a, side projections). However, these layers have a different topology and

symmetry visible in frontal projections (Figures 2b and 4b). In sazhinite, the wollastonite chain multiplies into the ribbon by the mirror plane m_y (Figure 4b) and then into the layer by inversion centers valid only for the layer pairs and not for the whole structure. That corresponds to local symmetry operation used in OD theory. A flat ribbon is formed in sazhinite in contrast to a double-decker ribbon in new silicate and in $K_3Eu[Si_6O_{13}(OH)_4]\cdot 2H_2O$ because of influence of large K atoms [40]. The β-$K_3Nd[Si_6O_{15}]$ [44] (Table 5) is a distorted variety of the sazhinite crystal structure (Figure 4a–d).
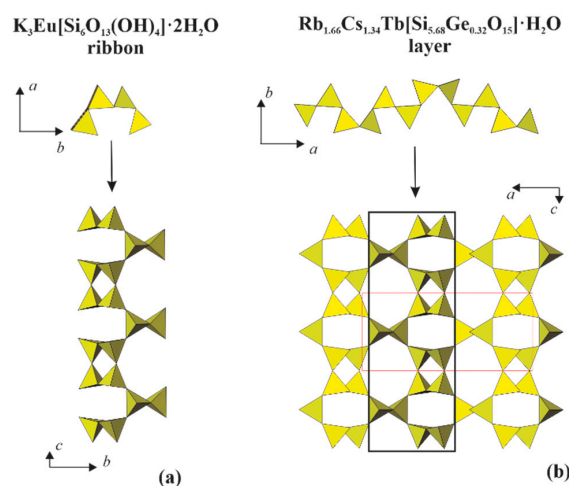

Figure 3. The ribbon in the crystal structure of $K_3Eu[Si_6O_{13}(OH)_4]\cdot 2H_2O$ (**a**) and the layer in the crystal structure of $Rb_{1.66}Cs_{1.34}Tb[Si_{5.43}Ge_{0.57}O_{15}]\cdot H_2O$ (**b**).
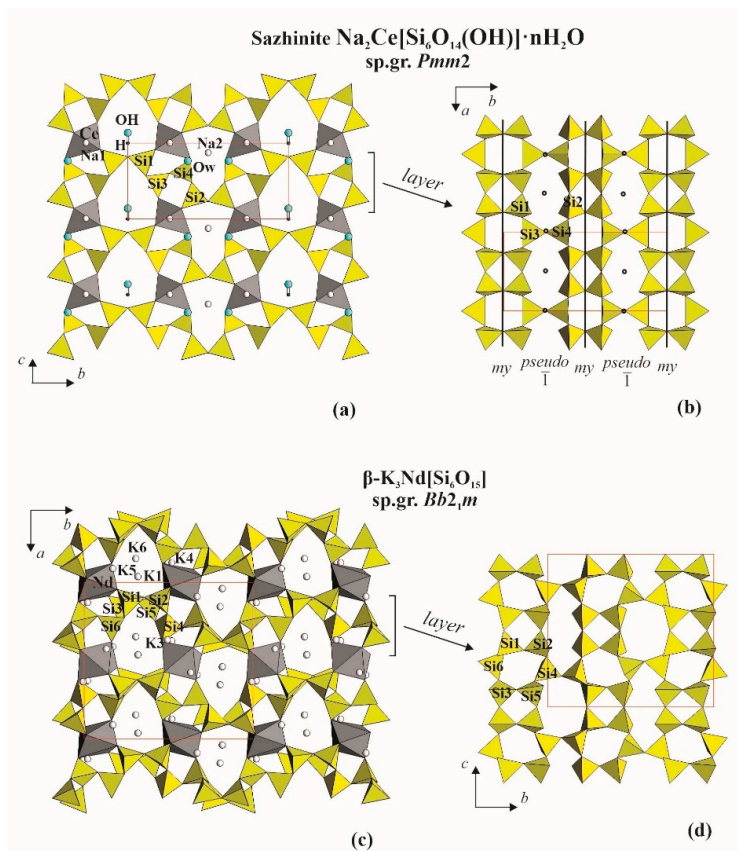

Figure 4. Crystal structure of sazhinite: mixed framework in *bc*-projection (**a**), Si-O tetrahedral layer in *ab*-projection (**b**); crystal structure of β-$K_3Nd[Si_6O_{15}]$: mixed framework in *ab*-projection (**c**), Si-O tetrahedral layer in *bc*-projection (**d**).

The original crystal structure $Na_{2.4}Ce[Si_6O_{15}]\cdot2H_2O$ [43] (Table 5, Figure 5) discussed in [40] has a new variant multiplication of wollastonite chains into the ribbon by a_z glide which are further multiplied by the inversion center in the layer.

Na$_{2.4}$Ce[Si$_6$O$_{15}$]·2H$_2$O
sp.gr. *Pmna*
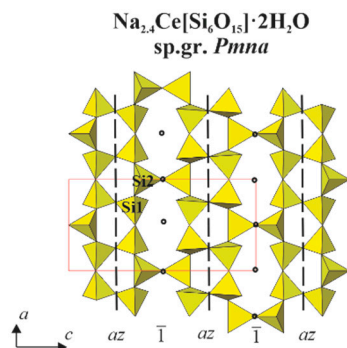
Figure 5. Si-O tetrahedral layer of $Na_{2.4}Ce[Si_6O_{15}]\cdot2H_2O$ crystal structure in *ac*-projection.

In the $NaNd[Si_6O_{13}(OH)_2]\cdot H_2O$ [48] (equal to $Na_3Nd[Si_6O_{15}]\cdot2H_2O$ [49]), $Na_{2.74}K_{0.26}$ $Ce[Si_6O_{15}]\cdot2H_2O$, $Na_3La[Si_6O_{15}]\cdot2.25H_2O$ and $Na_{2.72}K_{0.25}LaSi_6O_{15}\cdot2.25H_2O$ [42] crystal structures (Table 5, Figure 6a,b), two variants of ribbon-forming are observed: by m_x as in sazhinite, and by the b_x operation in accordance with the unit cell selection. Ribbons are connected into the layer by local operation or pseudo-inversion centers $\bar{1}$ (Figure 6b). As a result, the *a* parameter (*b* in sazhinite) is doubled (Table 5).

NaNd[Si$_6$O$_{13}$(OH)$_2$]·H$_2$O
sp.gr. *Cmm*2

(a)   **(b)**
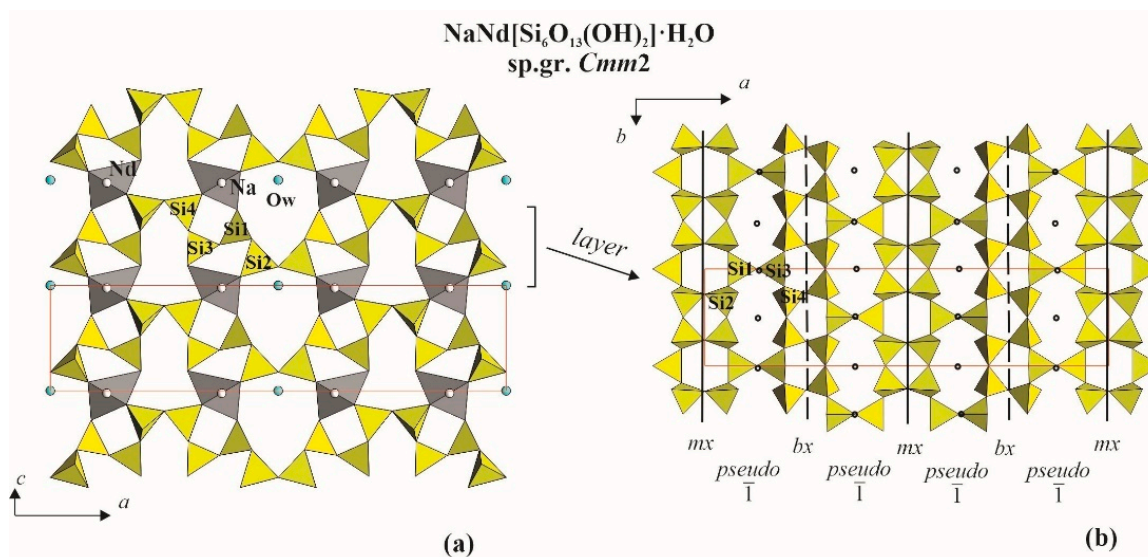
Figure 6. Crystal structure of $NaNd[Si_6O_{13}(OH)_2]\cdot H_2O$: mixed framework in *ac*-projection (**a**), Si-O tetrahedral layer in *ab*-projection (**b**).

4.2. Topology-Symmetry Analysis and Structure Prediction

Based on the topology-symmetry analysis of this family of layered crystal structures and the wollastonite chain with m_x symmetry, we can identify the ribbon from the chain by three variants of symmetry operations: m_y, $\bar{1}$ (equal to 2_x) and a_y. This first step is illustrated at the top of the Figure 7. The ribbons can be connected into the layers in several ways using the same operations: m_y, $\bar{1}$ and a_y left to right, shown on the next line marked as "layers". The first case is when the ribbon with the symmetry Pm_y is multiplied by the mirror plane m_y giving the layer with the polar symmetry group *Pmm*2. Multiplication of the same ribbon by the inversion center gives the layer of idealized sazhinite with symmetry group *Pmmb*. The second case is when a centro-symmetric ribbon with symmetry $P\bar{1}$ is multiplied

by m_y, giving the *Pmmb* space group or by the inversion center giving the *P2/m* space group. The third case describes multiplying of the ribbon with another symmetry group *Pa* by m_y or inversion center giving the *Cmm*2 or *Pman* space groups, correspondingly. The latter variant presents known structure $Na_{2.4}Ce[Si_6O_{15}]\cdot 2H_2O$ (space group setting *Pmna*) [43]. In all drawings, the resulting unit cells are shown.
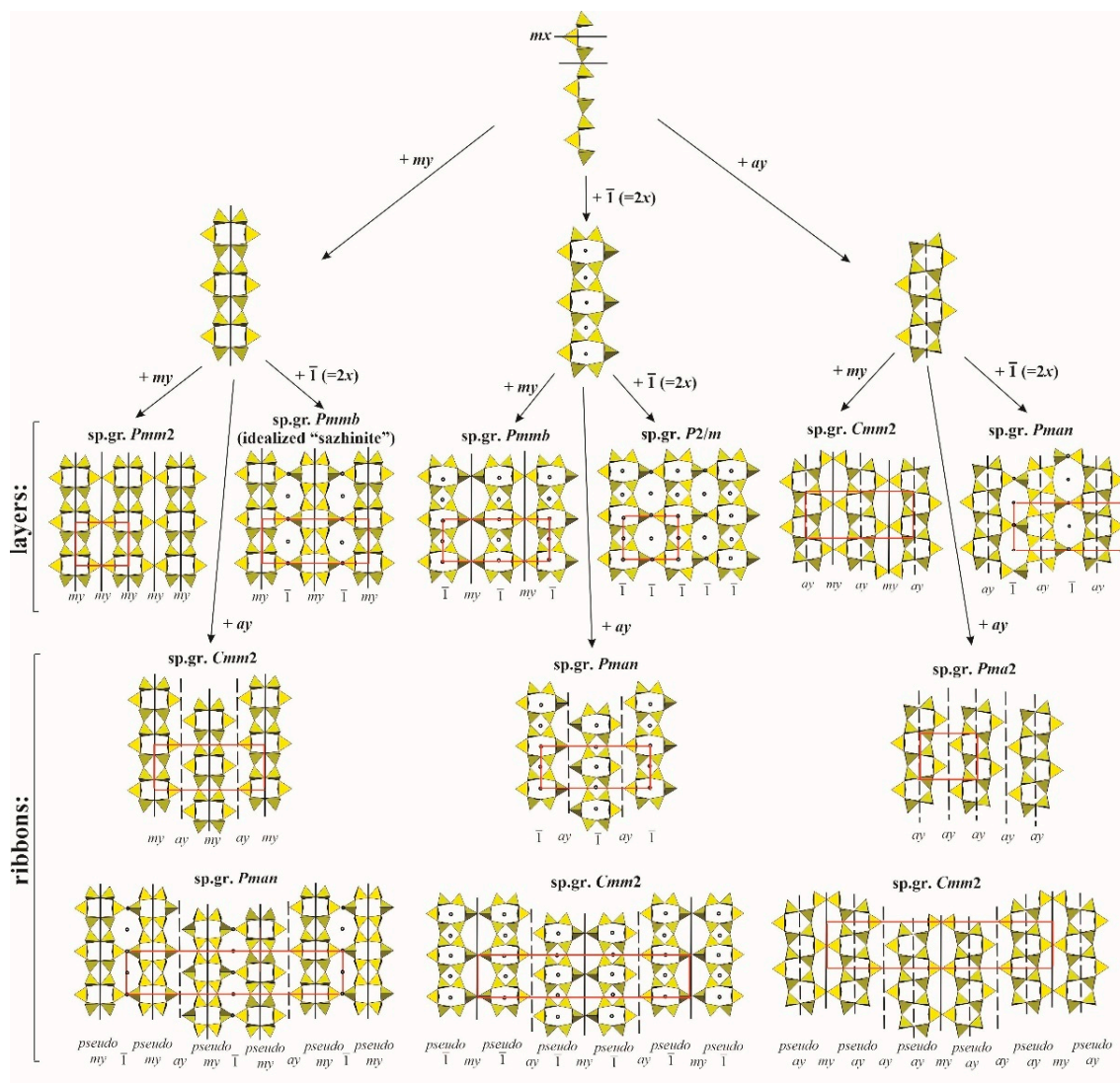

Figure 7. Construction of anionic Si-O radicals based on wollastonite chain and different multiplying symmetry operations.

Structural diversity has an OD character described by a symmetry groupoid. The chain, which has a one-dimensional periodicity, is multiplied in the ribbon in different ways; thus, a groupoid family symbol of lower rank is used as it was in [25] for borates:

$$P\,(m_x)\,1 \qquad \lambda\text{-PO,}$$

$$\overline{1}||m_y||a_y \qquad \sigma\text{-PO.}$$

Different ribbons are joined by different symmetrical operations in different layers, and that corresponds to the groupoid family symbol:

$$(Pmm2||P2/m||Pma2)\,1 \qquad \lambda\text{-PO,}$$

$$\overline{1}||m_y||a_y \qquad \sigma\text{-PO.}$$

All variants are shown in Figure 7 and belong to the members of the unify OD family with the maximum degree of order (MDO) because the λ-PO and σ-PO operations are the same for every layer, and all the ribbon pairs in the layer are equal.

Periodic crystal structures with the alternation of λ-PO and σ-PO may exist in the family up to disordered members if no order will be in initial λ-PO or σ-PO.

It is possible to predict not only layers but also different ribbons containing crystal structures, if we use a_y as σ-PO. They are shown in the next row in Figure 7 for different initial ribbon λ-PO (see arrows) with the different σ-PO multiplication and resulting space groups and unit cells. Hypothetic crystal structures with double ribbons are shown at the bottom of Figure 7 as an intermediate case between ribbon and layered crystal structures.

The specific diffraction effects described in [40] were explained by the polytypic nature of the compounds. This is consistent with the order–disorder (OD) nature of the crystal structures belonging to the OD family described using topology-symmetry analysis.

5. Conclusions

Crystals of $Rb_{1.66}Cs_{1.34}Tb[Si_{5.43}Ge_{0.57}O_{15}]·H_2O$ have been synthesized hydrothermally in a multi-component system at T = 280 °C and P = 100 atm and luminescence properties on the crystals were investigated. The crystal structure of new Rb,Cs,Tb-silicate-germanate with the isomorphic substitution in tetrahedra consists of corrugated layers $[Si_{5.43}Ge_{0.57}O_{15}]_{∞∞}$ which are connected with isolated TbO_6-octahedra into the mixed microporous framework. Larger than Na,K-atoms, Rb, Cs atoms and water molecules fill the channels of the framework. The substitution of larger Nd, Eu REE by smaller Tb REE does not changes the dimensions of voids. Structural comparison with the related layered silicates was carried out. Modular description added with the symmetry analysis of the OD approach allows to systematically describe the structural families or to predict new members. Topology-symmetry analysis of this silicates family was performed based on consideration of the wollastonite chain and symmetry variants of chain combination into the ribbons and then into the layers. The structural representatives of minerals and synthetic compounds are potentially extended. One example of "hypothetical structure" with the space group *Pman* corresponds to real $Na_{2.4}Ce[Si_6O_{15}]·2H_2O$ being in a systematically derived position in the field of structural variants. Most of the hypothetical layered and ribbon crystal structures are not yet discovered. Their description will help to recognize new crystal structures of minerals in nature or in synthetic experiments and to confirm the predicted models.

References

1. Mineralogy Database. Available online: http://www.mindat.org/ (accessed on 20 October 2020).
2. ICSD FIZ. Available online: http://www.fiz-karlsruhe.de (accessed on 20 October 2020).
3. Crystallography Open Database. Available online: http://www.crystallography.net (accessed on 20 October 2020).
4. Garra, W.; Marchetti, F.; Merlino, S. Tb/Na tobermorite: Thermal behaviour and high temperature products. *J. Solid State Chem.* **2009**, *182*, 1529–1532. [CrossRef]

5. Wierzbicka-Wieczorek, M.; Göckeritz, M.; Kolitsch, U.; Lenz, C.; Giester, G. Crystallographic and Spectroscopic Investigations on Nine Metal-Rare-Earth Silicates with the Apatite Structure Type. *Eur. J. Inorg. Chem.* **2015**, *2015*, 948–963. [CrossRef]

6. Latshaw, A.M.; Wilkins, B.O.; Hughey, K.D.; Yeon, J.; Williams, D.E.; Tran, T.T.; Halasyamani, P.S.; Loye, H.-C.Z. A 5 RE 4 X [TO 4] 4 crystal growth and photoluminescence. Fluoride flux synthesis of sodium and potassium rare earth silicate oxyfluorides. *CrystEngComm* **2015**, *17*, 4654–4661. [CrossRef]

7. Fleet, M.E.; Liu, X. Rare earth disilicates R2Si2O7 (R = Gd, Tb, Dy, Ho): Type B. *Z. Krist. Cryst. Mater.* **2003**, *218*, 795–801. [CrossRef]

8. Vidican, I.; Smith, M.D.; Zur Loye, H.-C. Crystal growth, structure determination and optical properties of new potassi-um-rare-earth silicates K3RESi2O7 (RE = Gd, Tb, Dy, Ho, Er, Tm, Yb, Lu). *J. Solid St. Chem.* **2003**, *170*, 203–210. [CrossRef]

9. Sieke, C.; Hartenbach, I.; Schleid, T. Sulfidisch derivatisierte Oxodisilicate der schweren Lanthanide vom Formeltyp $M_4S_3(Si_2O_7)$ (M = Gd − Tm). *Z. Nat. B J. Chem. Sci.* **2002**, *B57*, 1427–1432.

10. Ananias, D.; Kostova, M.; Paz, F.A.A.; Ferreira, A.; Carlos, L.D.; Klinowski, J.; Rocha, J. Photoluminescent Layered Lanthanide Silicates. *J. Am. Chem. Soc.* **2004**, *126*, 10410–10417. [CrossRef]

11. Fulle, K.; Sanjeewa, L.D.; McMillen, C.D.; Kolis, J.W. Crystal chemistry and the role of ionic radius in rare earth tetrasilicates: $Ba_2RE_2Si_4O_{12}F_2$(RE = Er^{3+}–Lu^{3+}) and $Ba_2RE_2Si_4O_{13}$(RE = La^{3+}–Ho^{3+}). *Acta Crystallogr. Sect. B Struct. Sci. Cryst. Eng. Mater.* **2017**, *73*, 907–915. [CrossRef]

12. Topnikova, A.P.; Belokoneva, E.L.; Dimitrova, O.V.; Volkov, A.S.; Nelyubina, Yu.V. $Na_3Tb_3[Si_6O_{18}]\cdot H_2O$, a synthetic analogue of microporous mineral gerenite. *Cryst. Rep.* **2016**, *61*, 566–570. [CrossRef]

13. Lee, C.-S.; Liao, Y.-C.; Hsu, J.-T.; Wang, S.-L.; Lii, K.-H. $Rb_2REGaSi_4O_{12}$ (RE = Y, Eu, Gd, Tb): Luminescent Mixed-Anion Double Layer Silicates Containing Chains of Edge-Sharing REO_7 Pentagonal Bipyramids. *Inorg. Chem.* **2008**, *47*, 1910–1912. [CrossRef]

14. Bao, X.; Liu, X.; Liu, X. High-pressure synthesis, crystal structure and photoluminescence properties of a new terbium silicate: $Na_2Tb_{1.08}Ca_{2.92}Si_6O_{18}H_{0.8}$. *RSC Adv.* **2017**, *7*, 50195. [CrossRef]

15. Wang, G.; Li, J.; Yu, J.; Chen, P.; Pan, Q.; Song, H.; Xu, R. $Na_3TbSi_3O_9\cdot3H_2O$: A New Luminescent Microporous Terbium(III) Silicate Containing HelicalSechserSilicate Chains and 9-Ring Channels. *Chem. Mater.* **2006**, *18*, 5637–5639. [CrossRef]

16. Morrison, G.; Latshaw, A.M.; Spagnuolo, N.R.; Loye, H.-C.Z. Observation of Intense X-ray Scintillation in a Family of Mixed Anion Silicates, $Cs_3RESi_4O_{10}F_2$(RE = Y, Eu–Lu), Obtained via an Enhanced Flux Crystal Growth Technique. *J. Am. Chem. Soc.* **2017**, *139*, 14743–14748. [CrossRef]

17. Taroev, V.K.; Kashaev, A.A.; Malcherek, T.; Goettlicher, J.; Kaneva, E.V.; Vasiljev, A.D.; Suvorova, L.F.; Suvorova, D.S.; Tauson, V.L. Crystal structures of new potassium silicates and aluminosilicates of Sm, Tb, Gd, and Yb and their relation to the armstrongite $(CaZr(Si_6O_{15})\cdot3H_2O)$ structure. *J. Solid State Chem.* **2015**, *227*, 196–203. [CrossRef]

18. Zhao, X.; Li, J.; Chen, P.; Li, Y.; Chu, Q.; Liu, X.; Yu, J.; Xu, R. New Lanthanide Silicates Based on Anionic Silicate Chain, Layer, and Framework Prepared under High-Temperature and High-Pressure Conditions. *Inorg. Chem.* **2010**, *49*, 9833–9838. [CrossRef] [PubMed]

19. Ananias, D.; Ferreira, A.; Rocha, J.; Ferreira, P.; Rainho, J.P.; Morais, C.; Carlos, L.D. Novel Microporous Europium and Ter-bium Silicates. *J. Am. Chem. Soc.* **2001**, *123*, 5735–5742. [CrossRef] [PubMed]

20. Liebau, F. *Structural Chemistry of Silicates: Structure, Bonding, and Classification*; Springer: Berlin/Heidelberg, Germany, 1985; 347p.

21. Pushcharovsky, D.Y. *Structural Mineralogy of Silicates and Their Synthetic Analogues*; Nedra: Moscow, Russia, 1986; 160p.

22. Ferraris, G.; Makovicky, E.; Merlino, S. *Crystallography of Modular Materials*; Oxford University Press (OUP): Oxford, UK, 2008.

23. Dornberger-Schiff, K. *Grundzuege Einer Theorie der OD-Strukturen aus Schichten*; Deutsche Akademie der Wissenschaften, Berlin, Abhandlungen, Klasse fur Chemie, Geologie and Biologie: Halle, Germany, 1964; Volume 3, pp. 1–106.

24. Merlino, S. OD Structures in Mineralogy. *Per. Mineral.* **1990**, *59*, 69–92.

25. Belokoneva, E.L. Borate crystal chemistry in terms of the exnteded OD theory: Topology and symmetry analysis. *Cryst. Rev.* **2005**, *11*, 151–198. [CrossRef]

26. Ivanova, A.G.; Belokoneva, E.L.; Dimitrova, O.V. New condensed acid diborate $GdH[B_2O_5]$ with chain radical $[B2\square B2\Delta O10]8-]\infty$: Synthesis and crystal structure; diborates and their structural system in terms of OD theory. *Russ. J. Inorg. Chem.* **2004**, *49*, 816–822.

27. Belokoneva, E.L.; Reutova, O.V.; Dimitrova, O.V.; Volkov, A.S. Germanosilicate $Cs_2In_2[(Si_{2.1}Ge_{0.9})_2O_{15}](OH)_2\cdot H_2O$ with a New Corrugated Tetrahedral Layer: Topological Symmetry-Based Prediction of Anionic Radicals. *Crystallogr. Rep.* **2020**, *65*, 566–572. [CrossRef]

28. Dorenbos, P. Exchange and crystal field effects on the 4fn 15d levels of Tb3. *J. Phys. Condens. Matter* **2003**, *15*, 6249–6268. [CrossRef]

29. Pisarski, W.A.; Zur, L.; Sołtys, M.; Pisarska, J. Terbium-terbium interactions in lead phosphate glasses. *J. Appl. Phys.* **2013**, *113*, 143504. [CrossRef]

30. Berdowski, P.A.M.; Lammers, M.J.J.; Blasse, G. 5D3-5D4 cross-relaxation of Tb^{3+} in α-GdOF. Chem. *Phys. Lett.* **1985**, *113*, 387–390.

31. Van Uitert, L.G.; Johnson, L.F. Energy Transfer between Rare—Earth Ions. *J. Chem. Phys.* **1966**, *44*, 3514. [CrossRef]

32. Tonooka, K.; Nishimura, O. Spectral changes of Tb^{3+} fluorescence in borosilicate glasses. *J. Lumin.* **2000**, *87*, 679–681. [CrossRef]

33. Deyneko, D.V.; Morozov, V.A.; Vasin, A.A.; Aksenov, S.M.; Dikhtyar, Y.Y.; Stefanovich, S.Y.; Lazoryak, B.I. The crystal site engineering and turning of cross-relaxation in green-emitting β-$Ca_3(PO_4)_2$-related phosphors. *J. Lumin.* **2020**, *223*, 117196. [CrossRef]

34. *CrysAlis PRO*; Agilent Technologies Ltd.: Yarnton, Oxfordshire, UK, 2014.

35.   Sheldrick, G.M. A short history of SHELX. *Acta Cryst.* **2008**, *64*, 112–122. [CrossRef] [PubMed]

36.   Farrugia, L.J. WinGX and ORTEP for Windows: An update. *J. Appl. Cryst.* **2012**, *45*, 849. [CrossRef]

37.   Pauling, L. *The Nature of the Chemical Bond*; Cornell University: Ithaca, NY, USA, 1960; 644p.

38.   Sheldrik, G.M. Crystal structure refinement with SHELXL. *Acta Cryst.* **2015**, *71*, 3–8.

39.   Dowty, E. *ATOMS*; Shape Software: Kingsport, TN, USA, 2006.

40.   Cadoni, M.; Ferraris, J. Polytypic and polymorphic relations between sazhinite and isochemical alkali-REE layer silicates. *Eur. J. Mineral.* **2011**, *23*, 85–90. [CrossRef]

41.   Shumyatskaya, N.G.; Voronkov, A.A.; Pyatenko, Yu.A. Sazhinite $Na_2Ce[Si_6O_{14}(OH)] \cdot nH_2O$, a new member of crystal chemical family of dalyite. *Sov. Phys. Cryst.* **1980**, *25*, 728–734.

42.   Cadoni, M.; Cheah, Y.L.; Ferraris, G. New RE microporous heteropolyhedral silicates containing 41516182 tetrahedral sheets. *Acta Crystallogr. Sect. B Struct. Sci.* **2010**, *66*, 158–164. [CrossRef] [PubMed]

43.   Jeong, H.-K.; Chandrasekaran, A.; Tsapatsis, M. Synthesis of a new open framework cerium silicate and its structure determination by single crystal X-ray diffraction. *Chem. Commun.* **2002**, 2398–2399. [CrossRef] [PubMed]

44.   Haile, S.M.; Wuensch, B.J. Structure, phase transitions and ionic conductivity of $K_3NdSi_6O_{15} \cdot xH_2O$. II. Structure of β-$K_3NdSi_6O_{15}$. *Acta Cryst.* **2000**, *56*, 349–362. [CrossRef]

45.   Pushcharovsky, D.Y.; Karpov, O.G.; Pobedimskaya, E.A.; Belov, N.V. Crystal structure of $K_3NdSi_6O_{15}$. *Dokl. AN SSSR* **1977**, *234*, 1323–1326.

46.   Rastsvetaeva, R.K.; Aksenov, S.M.; Taroev, V.K. Crystal Structures of Endotaxic Phases in Europium Potassium Silicate Having a Pellyite Unit Cell. *Crystallogr. Rep.* **2010**, *55*, 1041–1049. [CrossRef]

47.   Cámara, F.; Ottolini, L.; Devouard, B.; Garvie, L.A.J.; Hawthorne, F.C. Sazhinite-(La), $Na_3LaSi_6O_{15}(H_2O)_2$, a new mineral from the Aris phonolite, Namibia: Description and crystal structure. *Miner. Mag.* **2006**, *70*, 405–418. [CrossRef]

48.   Karpov, O.G.; Pushcharovsky, D.Y.; Pobedimskaya, E.A.; Burshtein, I.F.; Belov, N.V. Crystal structure of rare earth silicate $NaNdSi_6O_{13}(OH)_2 \cdot nH_2O$. *Dokl. AN SSSR* **1977**, *236*, 593–596.

49.   Haile, S.M.; Wuensch, B.J.; Laudise, R.A.; Maier, J. Structure of $Na_3NdSi_6O_{15} \cdot 2H_2O$—A Layered Silicate with Paths for Possible Fast-Ion Conduction. *Acta Cryst.* **1997**, *53*, 7–17. [CrossRef]